Supporting Information

Predicting binding affinities for GPCR ligands using free energy perturbation

Eelke B. Lenselink,[1] Julien Louvel,[1] Anna F. Forti,[1] Jacobus P. D. van Veldhoven,[1] Henk de Vries,[1] Thea Mulder-Krieger,[1] Fiona M. McRobb,[2] Ana Negri,[2]Joseph Goose,[2] Robert Abel,[2] Herman W. T van Vlijmen,[1] Lingle Wang,[2] Edward Harder,[2] Woody Sherman,[2] Adriaan P. IJzerman,[1] Thijs Beuming[2]**

1. Division of Medicinal Chemistry, Leiden Academic Centre for Drug Research, Leiden University, Leiden, The Netherlands

2. Schrödinger, Inc., 120 West 45th Street, New York, New York 10036, United States

Supplementary Methods

Default membrane relaxation protocol

The membrane relaxation protocol in the Schrödinger software was used to equilibrate the structure.[1] In total 8 refinement stages are used, two minimization stages for both 2000 steps, the first with restraints on the heavy atoms (50 kcal $mol^{-1}Å^{-1}$) and the second minimization stage without restraints, followed by two stages with a Gaussian shaped barrier potential.[2] The first stage gradually heated up the system from 0 to 310K in 60 ps, while lowering the restraints on heavy atoms from 50 kcal $mol^{-1}Å^{-1}$ to 10 kcal $mol^{-1}Å^{-1}$ using a Berendsen thermostat under NVT conditions. The second stage was run for 200 ps under NPT conditions with 10 kcal $mol^{-1}Å^{-1}$ restraints on heavy atoms. The last 4 stages, performed under NPT conditions were done as follows: 1) removing the Gaussian barrier potential for 100 ps applying 10 kcal $mol^{-1}Å^{-1}$ restraints on heavy atoms, 2) lowering the 10 kcal $mol^{-1}Å^{-1}$ restraints on heavy atoms to 2 kcal $mol^{-1}Å^{-1}$ during 600 ps, 3) 100 ps with 2 kcal $mol^{-1}Å^{-1}$ restraints on Cα atoms and 4) 100 ps of unrestrained simulation.

Additional Equilibration

An equilibration protocol was developed that was fully able to run on a GPU. It consists of 6 stages. In the first three stages the velocities are randomized every 1 ps, under Brownian NVT conditions. With a temperature of 10 K and 50 kcal $mol^{-1}Å^{-1}$ restraints on all heavy atoms in the first stage, which is simulated for 150 ps. Subsequently we lowered the restraints to 10 kcal $mol^{-1}Å^{-1}$ which was simulated at 150K in the second stage for 150 ps, and 2 kcal $mol^{-1}Å^{-1}$ restraints at 310 K in the last stage for 200 ps. The last three stages are performed under NPT conditions at 310K, with 1) 2 kcal $mol^{-1}Å^{-1}$ restraints on heavy atoms for 500 ps, 2) 500 ps with 2 kcal $mol^{-1}Å^{-1}$ restraints on Cα atoms, and 3) 1000 ps without any restraints.

Table S1. Predicted affinities of the different chiral compounds, for the adenosine A_{2A} receptor ($A_{2A}R$), Piersanti dataset.[3]

Receptor	Ligand	Experimental dG (kcal/mol)	Predicted dG (kcal/mol)
A_{2A}	14 (S)	-10.43	-11.02
A_{2A}	14 (R)	-10.43	-11.36
A_{2A}	15 (S)	-9.8	-9.99
A_{2A}	15 (R)	-9.8	-10.45

Table S2. Comparison between OPLS2.1[4] (used here for both retrospective and prospective studies) and the newer force field, OPLS3[5] for the five different datasets (retrospective only). Bold values are used for the cases were the MUE/hysteresis is better in OPLS2.1 than OPLS3 and *vice versa*. Moreover, the number of ligands and range of experimental affinities for the studied ligands is given. OPLS2.1 was compared with OPLS 3 based on the Mean Unsigned Error (MUE), which was calculated on the ΔΔG data.

Dataset/Receptor	No. of Ligands	Min/ Max. ΔG	MUE OPLS 2.1 (min/max)	MUE OPLS 3 (min/max)	Avg/max Hysteresis OPLS 2.1	Avg/max Hysteresis OPLS 3
Minetti et al.[6] Adenosine A_{2A}	9	-8.61/ -11.56	0.68 (0/2.52)	**0.64** (0.00/1.43)	0.68/2.28	**0.64**/2.05
Piersanti et al.[3] Adenosine A_{2A}	7	-9.80/ -11.07	**0.58** (0.05/1.44)	0.77 (0.04/1.46)	0.53/1.15	**0.43**/0.93
Thoma et al.[7] CXCR4 Chemokine	9	-6.81*/ -11.03	**1.56** (0.08/4.18)	1.62 (0.01/4.03)	1.79/4.34	**0.76**/2.02
Yuan et al.[8] δ-opioid	11	-9.57/ -12.85	**0.69** (0.06/1.72)	0.95 (0.03/2.78)	1.01/2.50	**1.00**/2.68
Christopher et al.[9] β1-adrenergic	9	-7.90/ -9.77	**1.08** (0.13/2.6)	1.46 (0.12/4.48)	0.82/3.08	**0.54**/2.25

Table S3. Predicted affinities for the 46 different proposed derivatives. For the compounds for which we performed extra perturbations (against all 7 Minetti ligands, see results) two affinities are reported. The first number is the predicted affinity when all perturbations are considered, the second number in parentheses is the predicted affinity where 2 perturbations are used (see main text). Compounds that were synthesized are indicated in bold, by compound numbers.

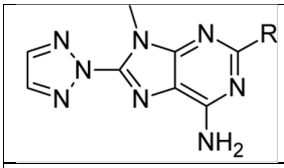

Virtual Compound (VC)/ Compound	**R- Group**	**Predicted ΔG (kcal/mol)**
VC-1	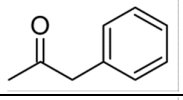	-11.47 ± 0.89
VC-2	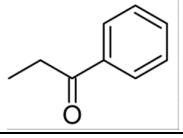	-11.24 ± 0.99
VC-3	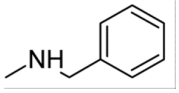	-11.35 ± 0.68
VC-4	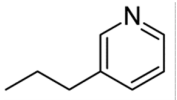	-11.08 ± 0.92
VC-5S	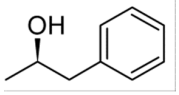	-11.38 ± 0.62
VC-5R	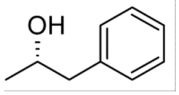	-11.99 ± 0.81
VC-6 **17**	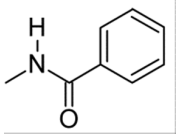	-12.87 ± 1.36 (-12.77 ± 1.18)
VC-7 **11**	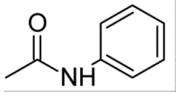	-12.89 ± 1.77 (-12.65 ± 0.89)
VC-8	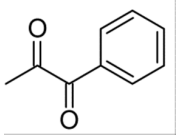	-12.97 ± 1.27 (-12.85 ± 0.76)

VC-9	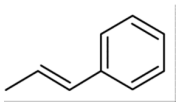	-11.63 ± 0.91
VC-10	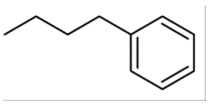	-11.73 ± 0.77
VC-11		-10.92 ± 0.94
VC-12	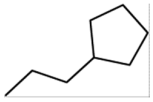	-11.98 ± 0.87 (-12.06 ± 0.68)
VC-13 **8**	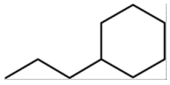	-11.90 ± 0.88 (-12.01 ± 0.68)
VC-14	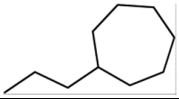	-11.56 ± 0.84
VC-15	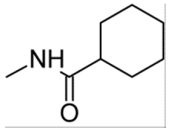	-10.94 ± 1.18
VC-16	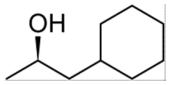	-11.95 ± 1.12
VC-17	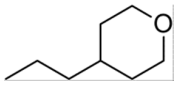	-10.71 ± 0.62
VC-18	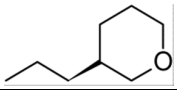	-10.87 ± 0.98
VC-19	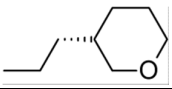	-11.52 ± 1.07
VC-20	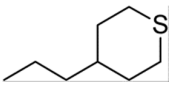	-11.23 ± 0.94
VC-21	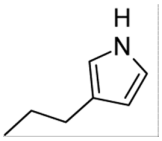	-10.27 ± 0.81
VC-22	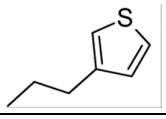	-11.40 ± 0.76
VC-23	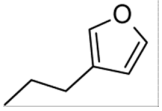	-11.27 ± 0.63

VC-24		-9.72 ± 0.65
VC-25	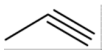	-10.83 ± 0.68
VC-26		-9.64 ± 0.86
VC-27	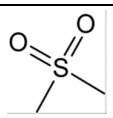	-10.33 ± 0.59
VC-28 **13**		-9.29 ± 0.47 (-9.37 ± 0.62)
VC-29	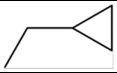	-10.29 ± 0.86
VC-30	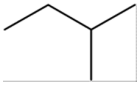	-10.24 ± 0.60
VC-31	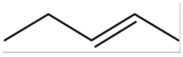	-10.65 ± 0.94
VC-32	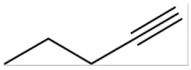	-10.80 ± 0.88
VC-33		-11.01 ± 0.86
VC-34	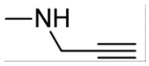	-11.03 ± 0.95
VC-35	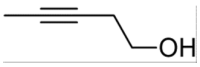	-11.66 ± 0.75
VC-36		-10.23 ± 0.62
VC-37	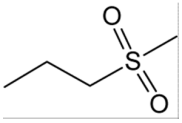	-10.35 ± 1.05
VC-38	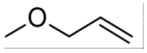	-10.50 ± 0.59
VC-39	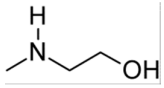	-11.26 ± 0.72
VC-40	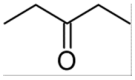	-10.25 ± 0.61
VC-41	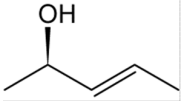	-11.40 ± 0.76
VC-42	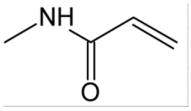	-10.63 ± 0.62

VC-43	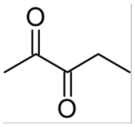	-12.07 ± 0.82
VC-44	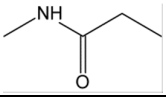	-11.30 ± 0.85
VC-45	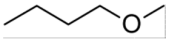	-10.33 ± 0.69
VC-46	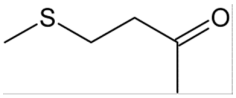	-10.59 ± 1.12

Ligand	Experimental ΔG (kcal/mol)	Predicted ΔG-4EIY (kcal/mol)	Predicted ΔG-3PWH (kcal/mol)	ΔΔG 4EIY-3PWH (kcal/mol)
1	-10.87	-8.98/-9.38/-10.02	-10.04/-10.25/-10.35	1.06/0.87/0.29
2	-8.24	-7.18/-7.55/-8.20	-9.10/-9.29/-9.35	1.92/1.75/1.15
3	-10.64	-10.29/-10.77/-11.06	-9.46/-9.48/-9.49	0.83/1.29/1.57
4	-12.16	-10.51/-9.38/-11.82	-11.00/-11.16/-11.22	0.49/1.78/0.60
5	-10.40	-12.40/-13.29/-	-10.62/-10.64/-	1.78/**2.65**/-
6	-8.31	-8.12/-8.46/-9.11	-9.67/-9.80/-9.86	1.55/1.34/0.75
7	-9.12	-12.26/-/-	-9.84/-/-	**2.42**/-/-
Average	-	-	-	1.44/1.61/0.87

Table S4. Predicted affinities and experimental ΔG for the compounds in Figure 2. Predicted ΔG of the different ligands for both crystal structures (4EIY and 3PWH) are shown. To test the dependency of prediction on the removal of unreliable perturbations, (based on the difference in predicted ΔG between 4EIY and 3PWH) first compound **7** was removed from the map and then ligand **5,** (indicated in bold). Affinities prior to removal, after removal of ligand **7**, and after removal of both ligand **5** and ligand **7** are reported (from left to right).

Figure S1. FEP map of the different perturbations, for the Minetti et al. compounds.[6] Arrows between compounds represent the different perturbations, blue values are the predicted ΔΔG (raw data) and black the experimental ΔΔG. Red arrows highlight bad perturbations, based on hysteresis.

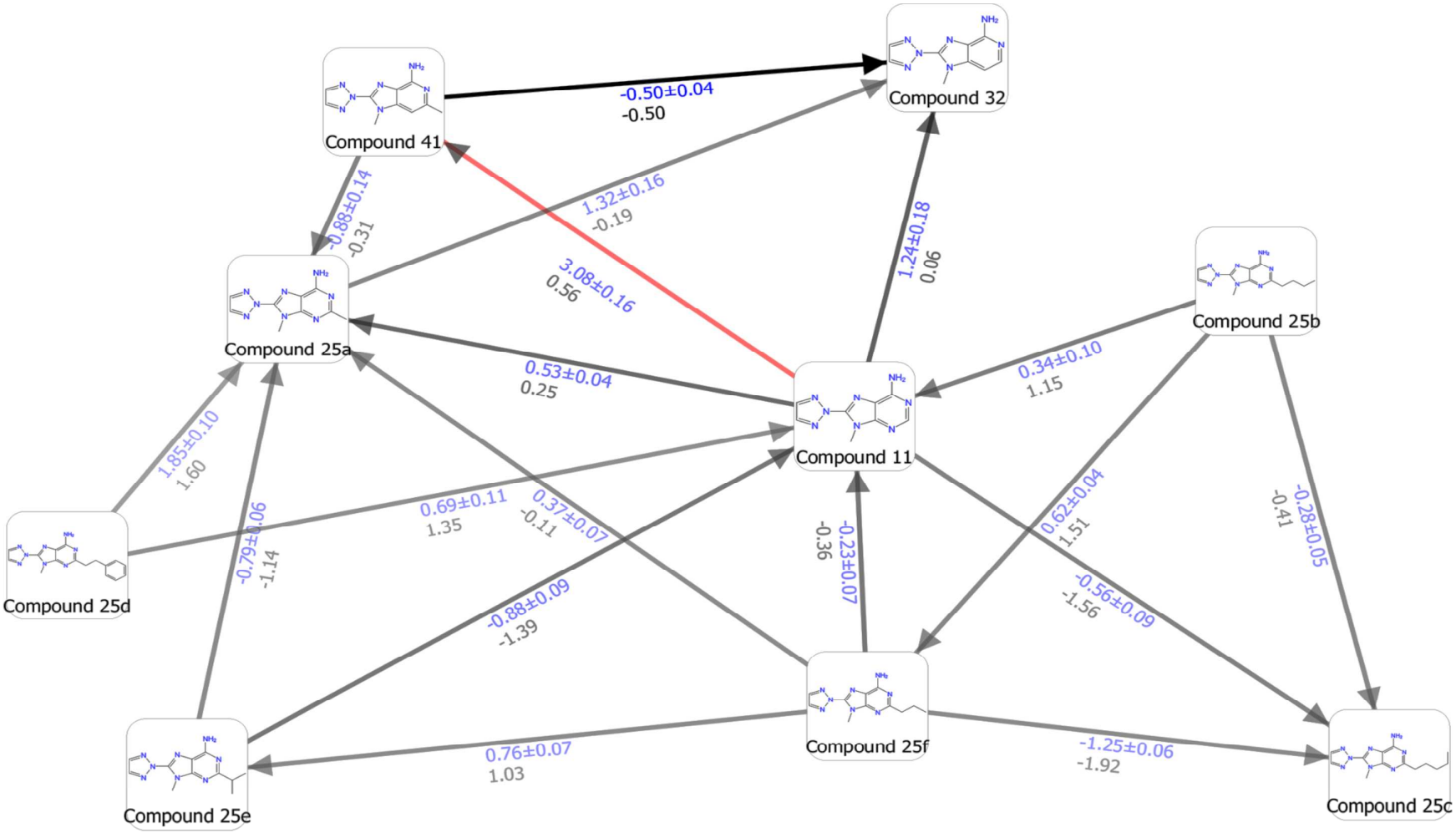

Figure S2. FEP map of the different perturbations, for the Piersanti et al. compounds.[3] Arrows between compounds represent the different perturbations. Blue values are the predicted ΔΔG (raw data) and black the experimental ΔΔG.

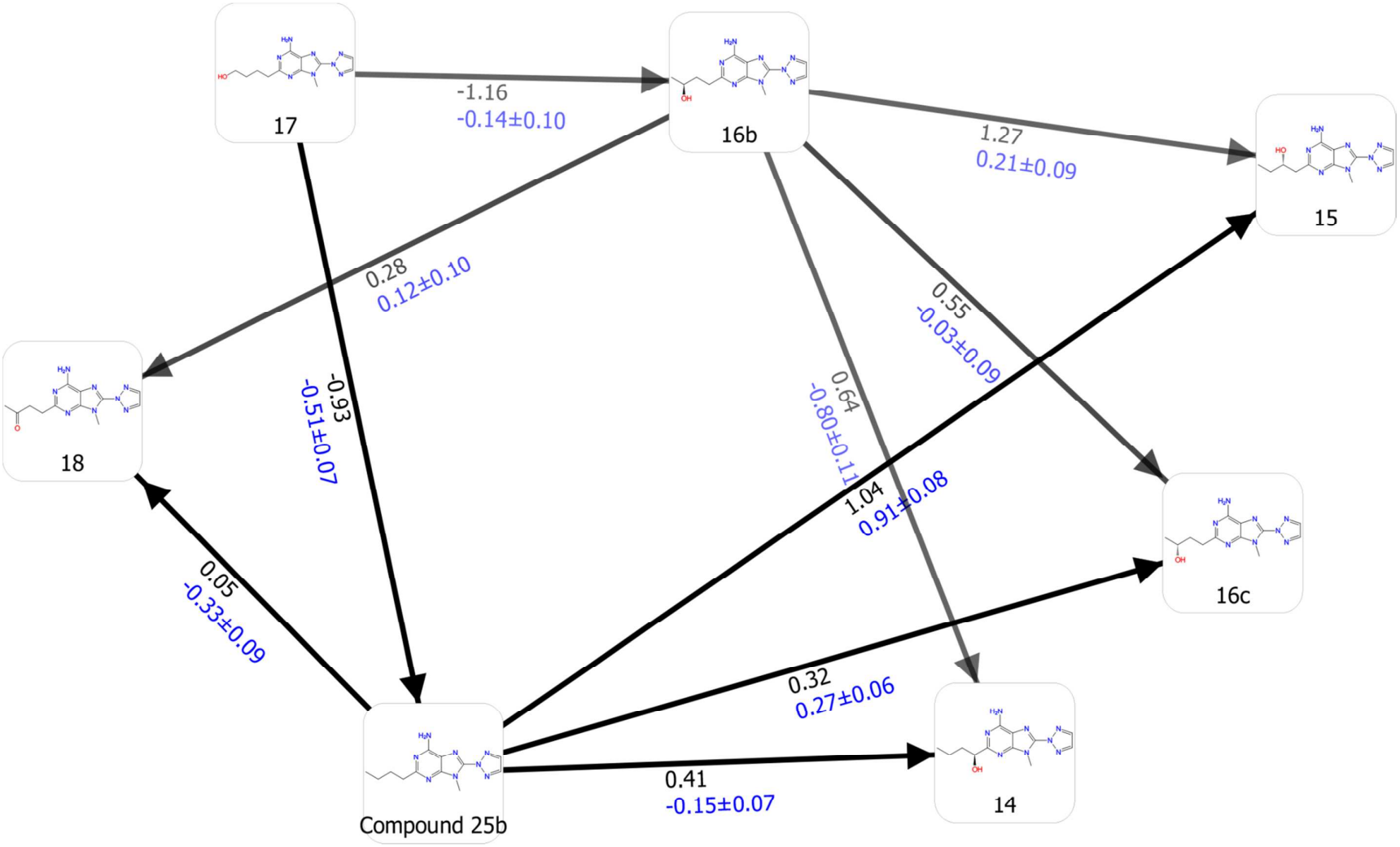

Figure S3. FEP map of the different perturbations, for the Christopher et al. compounds.[9] Arrows between compounds represent the different perturbations. Blue values are the predicted ΔΔG (raw data) and black the experimental ΔΔG. Red arrows highlight bad perturbations, based on hysteresis.

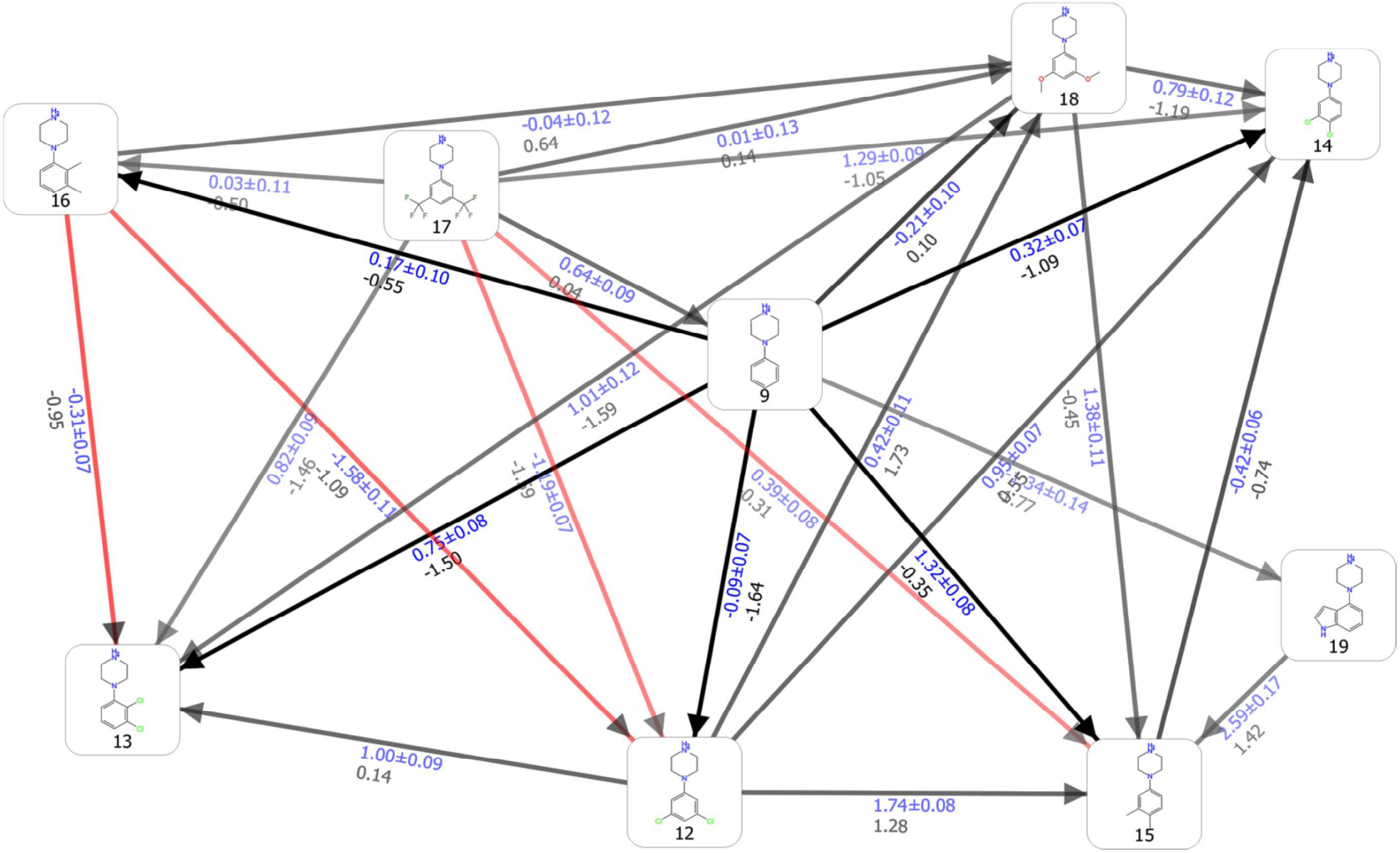

Figure S4. FEP map of the different perturbations, for the Yuan et al. compounds.[8] Arrows between compounds represent the different perturbations. Blue values are the predicted ΔΔG (raw data) and black the experimental ΔΔG. Red arrows highlight bad perturbations.

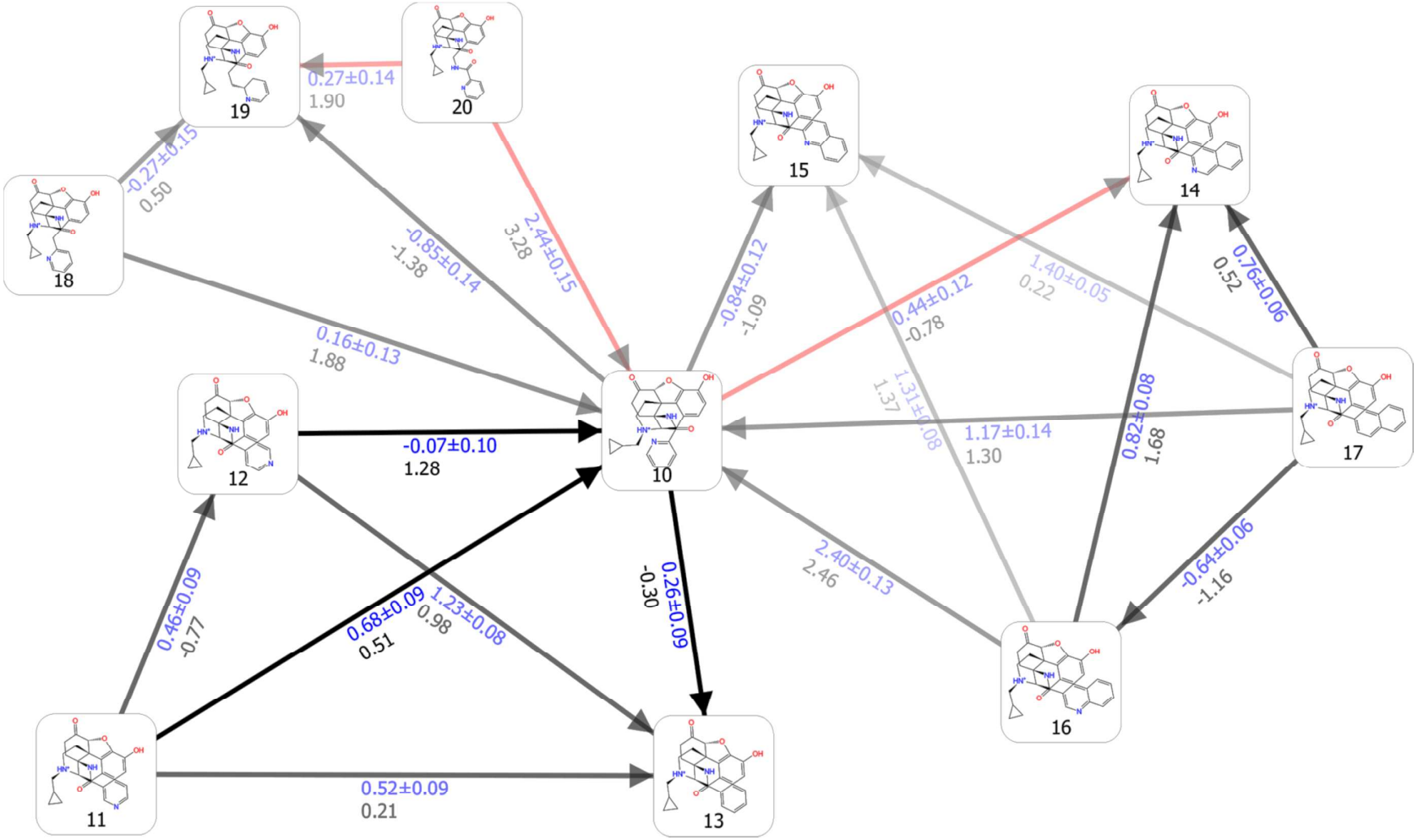

Figure S5. FEP map of the different perturbations, for the Thoma et al. compounds.[7] Arrows between compounds represent the different perturbations. Blue values are the predicted ΔΔG (raw data) and black the experimental ΔΔG. Red arrows highlight bad perturbations, based on hysteresis.

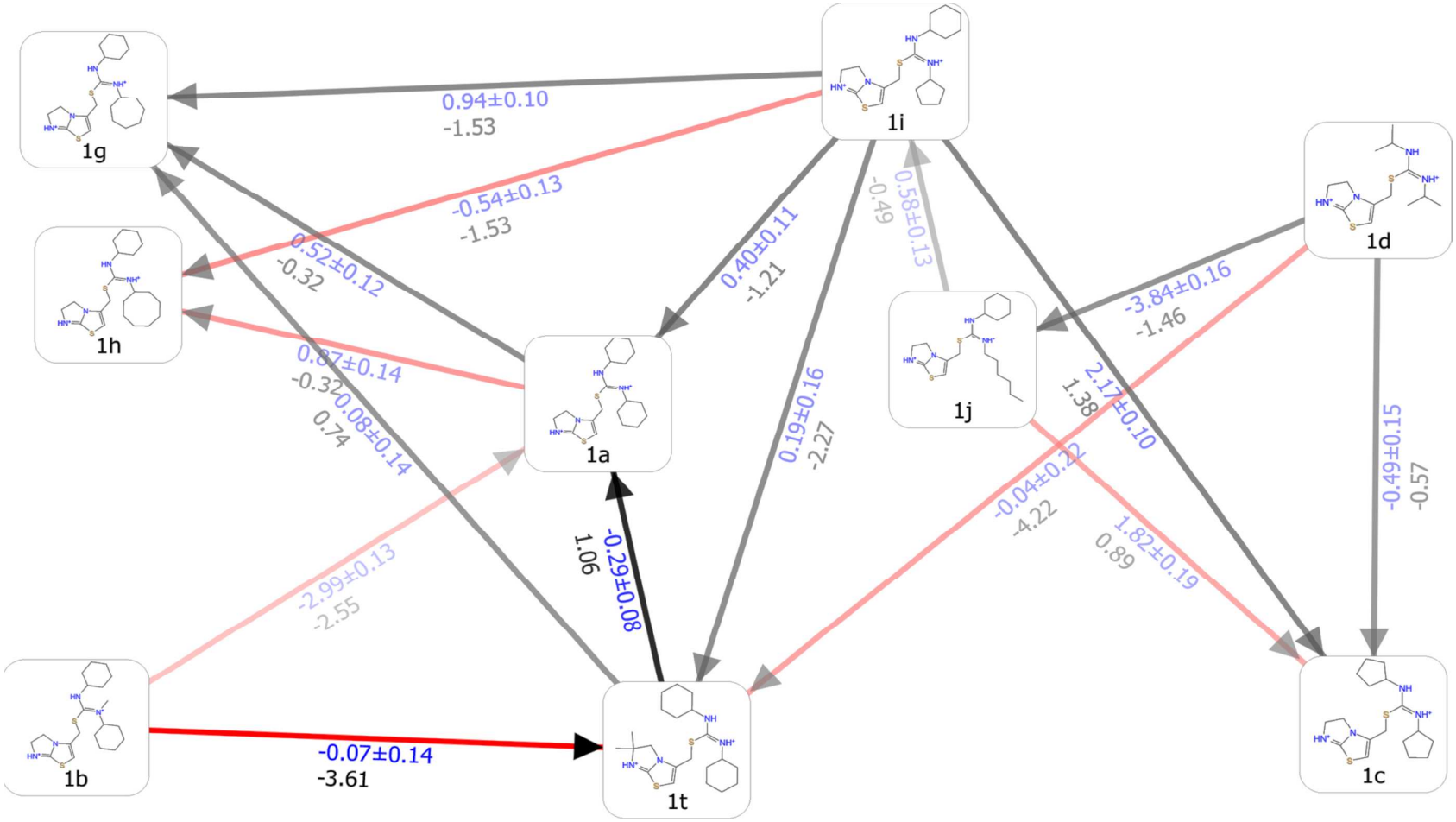

Figure S6. Scatter plot of the predicted ΔG of FEP+ versus the experimental ΔG, and the predicted ΔG of binding using MM-GBSA, for the Minetti et al. A_{2A} compounds.[6] For FEP+ the cycle closure error is given.

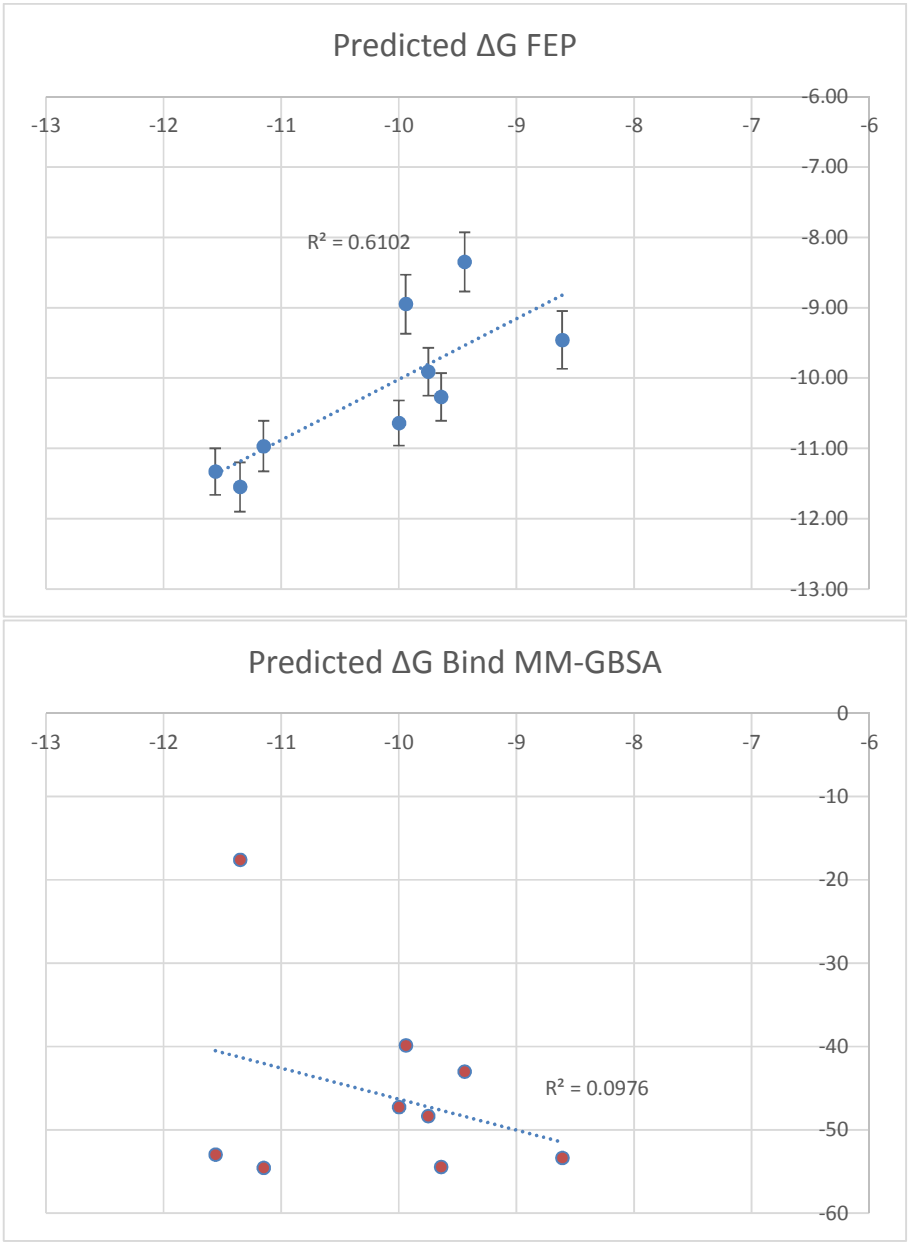

Figure S7. Scatter plot of the predicted ΔG of FEP+ versus the experimental ΔG, and the predicted ΔG binding using MM-GBSA, for the Piersanti et al. A_{2A} compounds.[3] For FEP+ the cycle closure error is given.

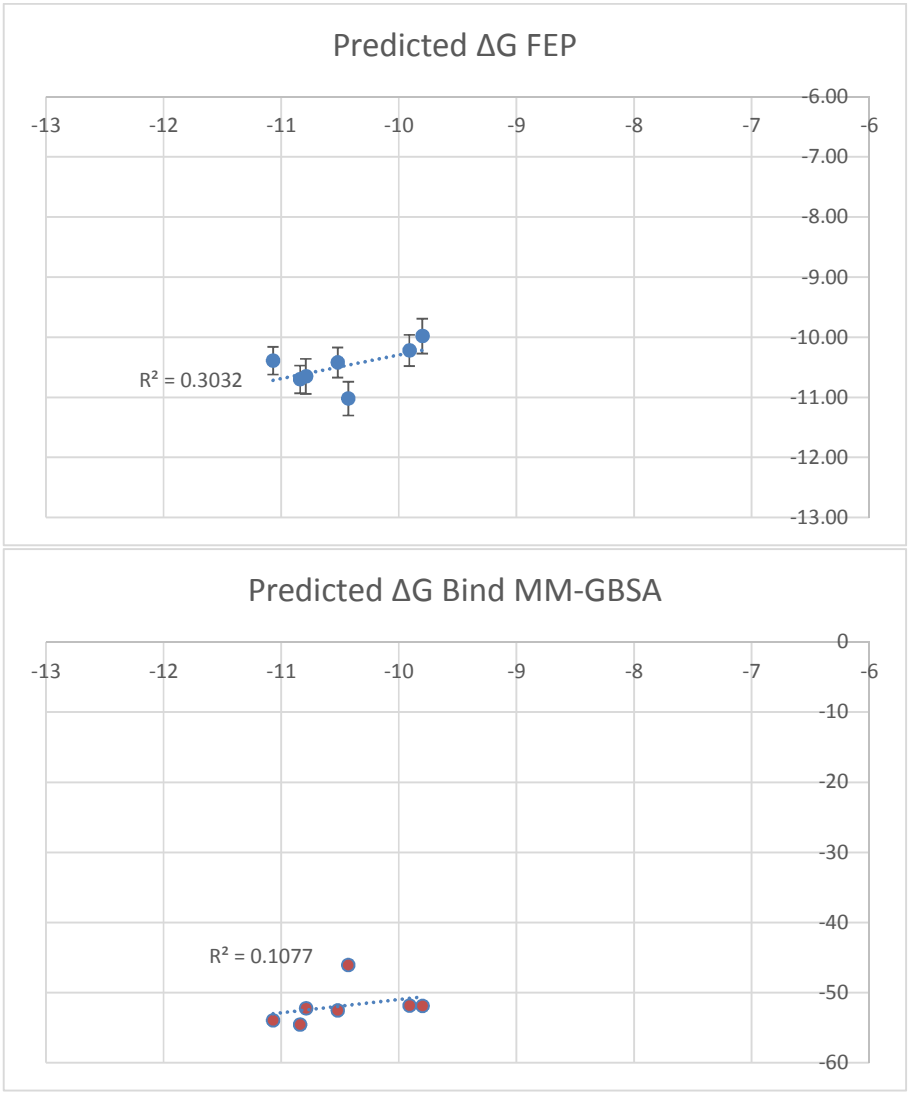

Figure S8. Scatter plot of the predicted ΔG of FEP+ versus the experimental ΔG, and the predicted ΔG binding using MM-GBSA, Christopher et al. B1AR compounds.[9] For FEP+ the cycle closure error is given.

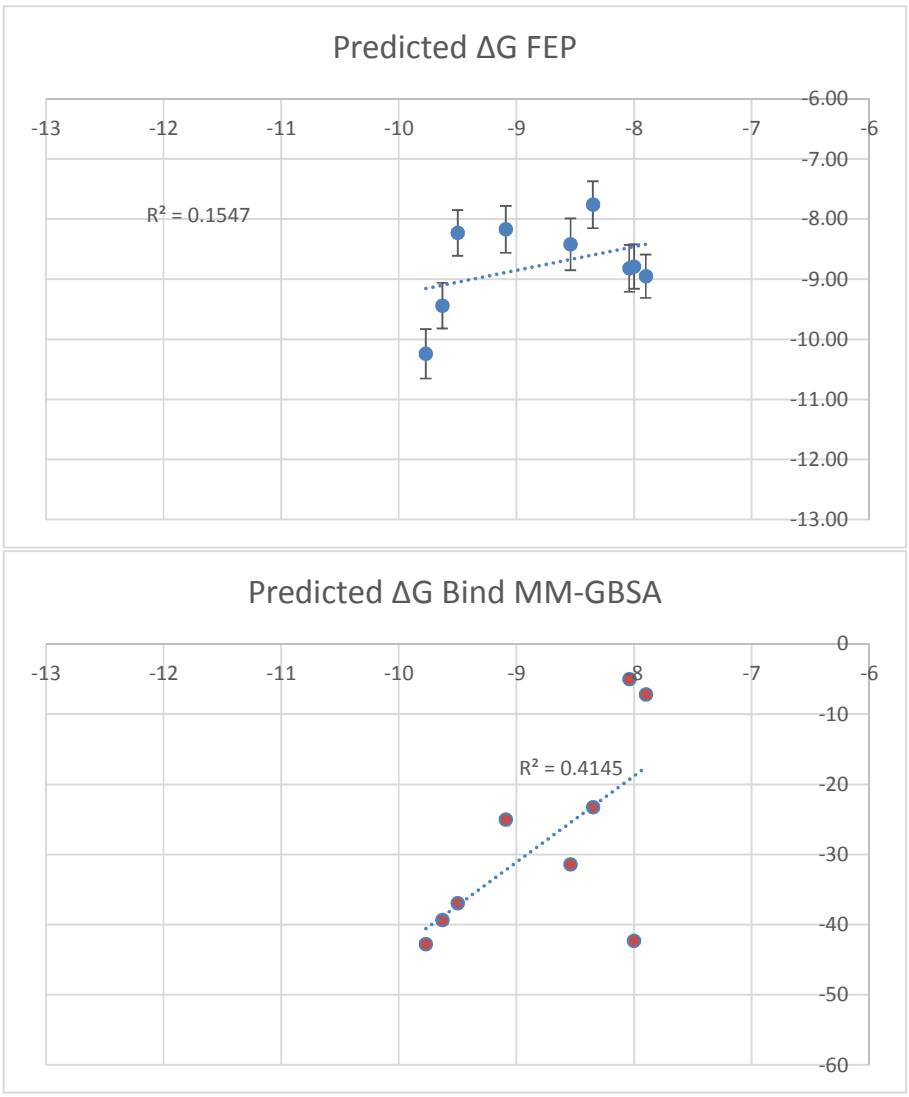

Figure S9. Scatter plot of the predicted ΔG of FEP+ versus the experimental ΔG, and the predicted ΔG binding using MM-GBSA, for the Yuan et al. DOR compounds.[8] For FEP+ the cycle closure error is given.

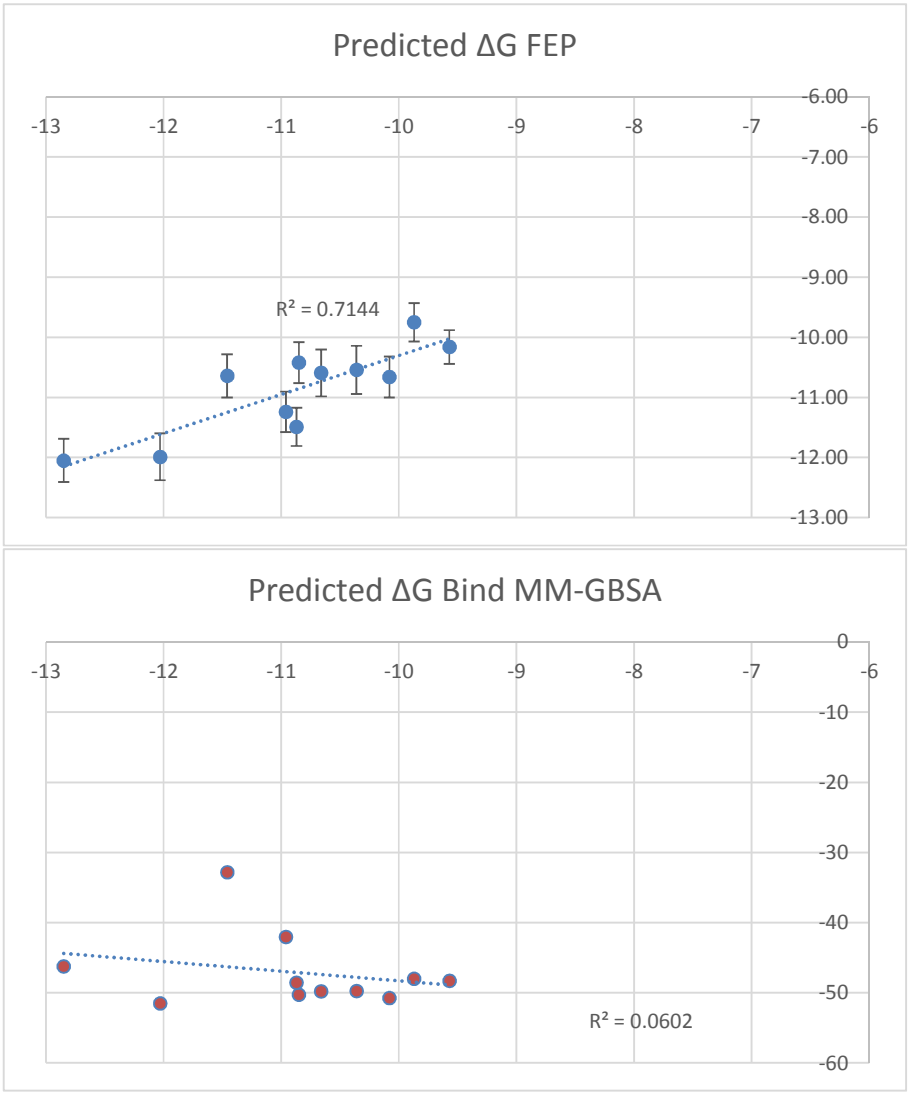

Figure S10. Scatter plot of the predicted ΔG of FEP+ versus the experimental ΔG, and the predicted ΔG binding using MM-GBSA, for the Thoma et al. CXCR4 compounds.[7] For FEP+ the cycle closure error is given.

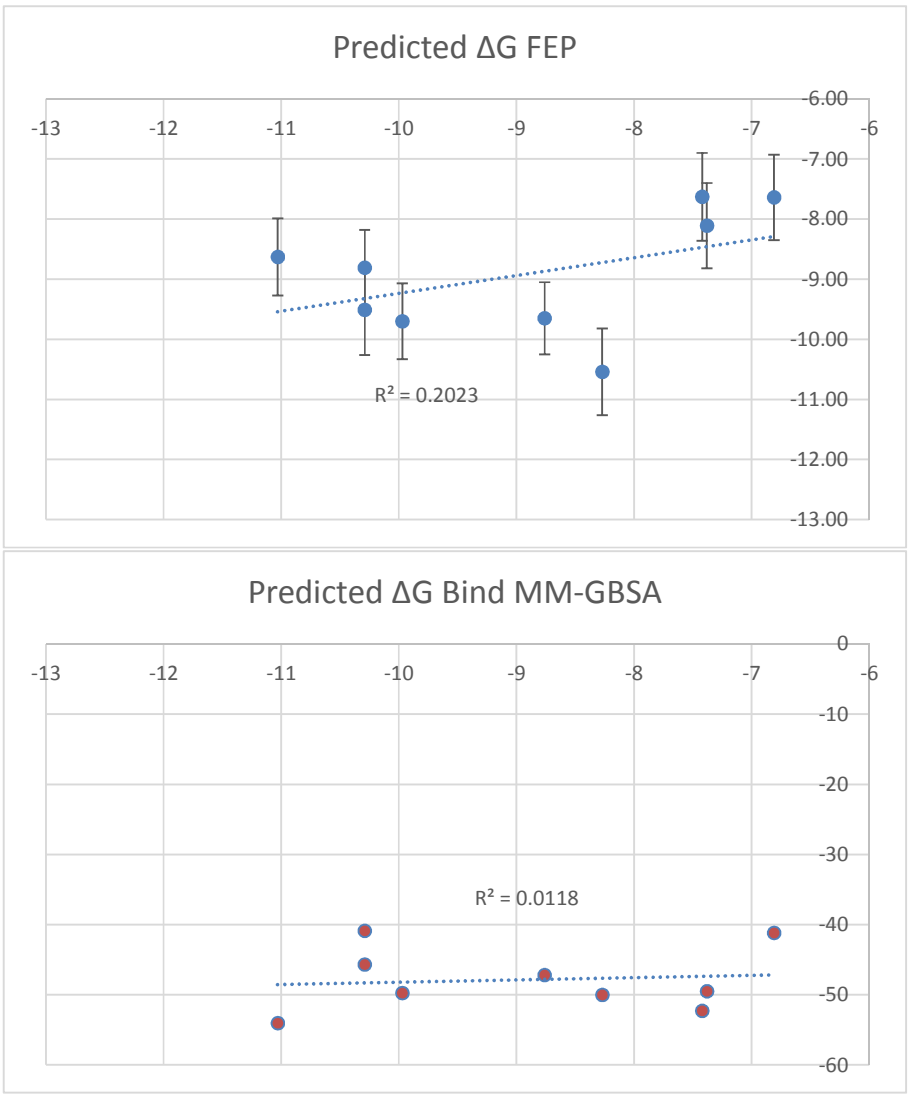

Figure S11. Full radioligand displacement curves and *Ki* values (n=3) for the different tested compounds: **3** (LUF7503), **2** (LUF7506), **1** (LUF7484), and **8** (LUF7510).

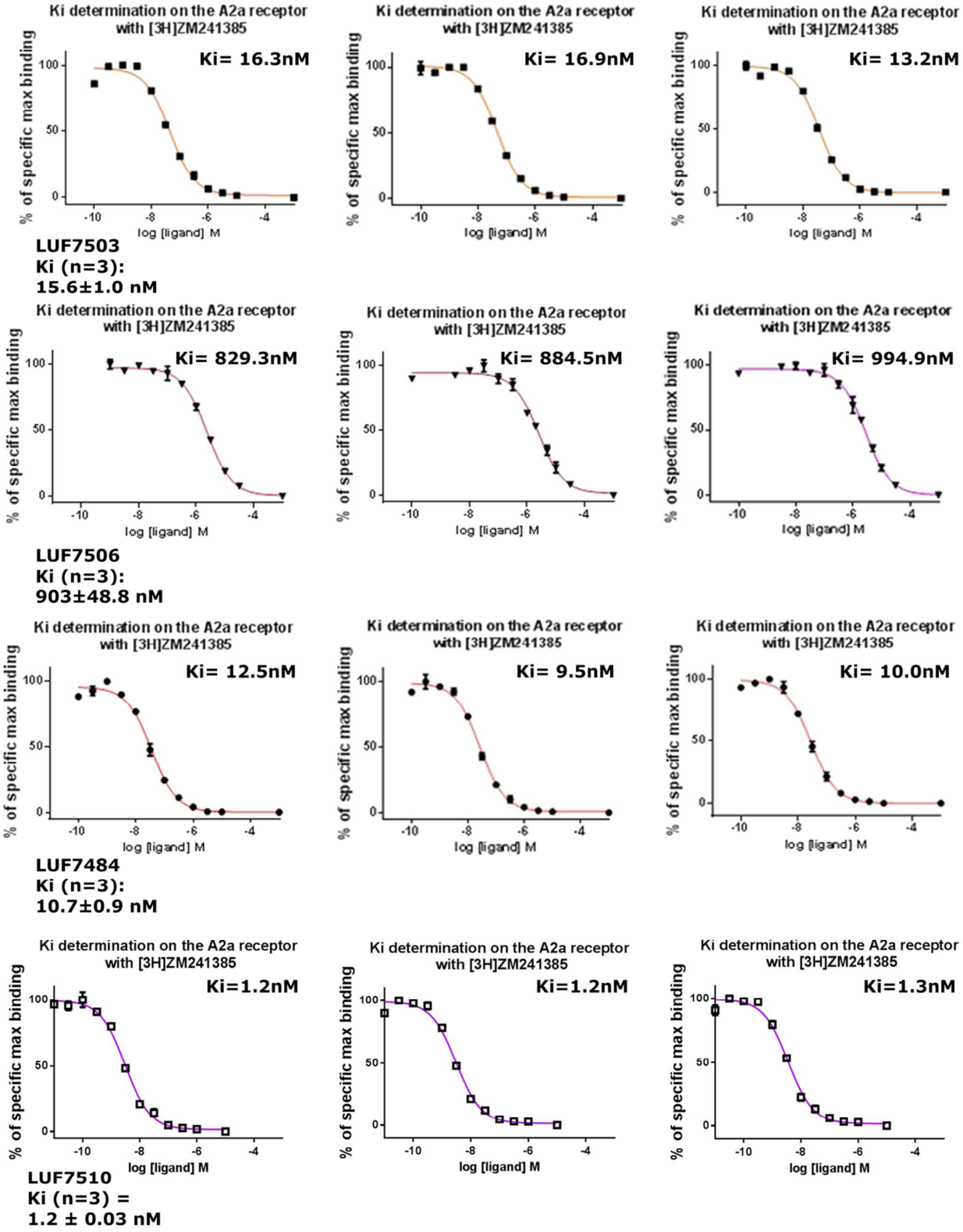

Figure S12. Full displacement curves and *Ki* (n=3) values for the different tested compounds: **13** (LUF7511), **17** (LUF7540), and **15** (LUF7555)

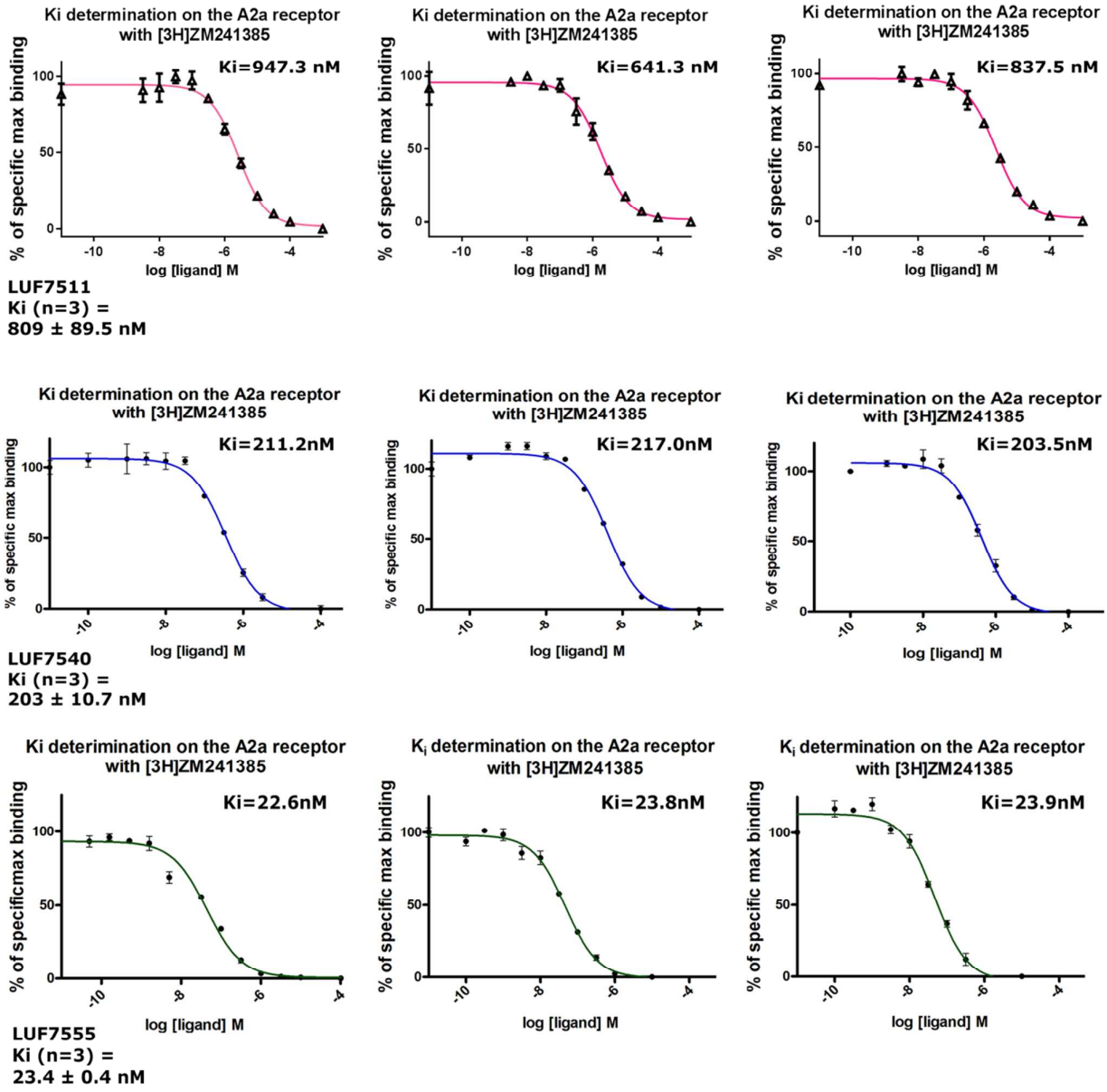

Figure S13. Structural difference between 4EIY and 3PWH. 4EIY is colored in green and 3PWH in orange. In 4EIY GLU169 and HIS264 form an ionic lock, in 3PWH this interaction is absent.

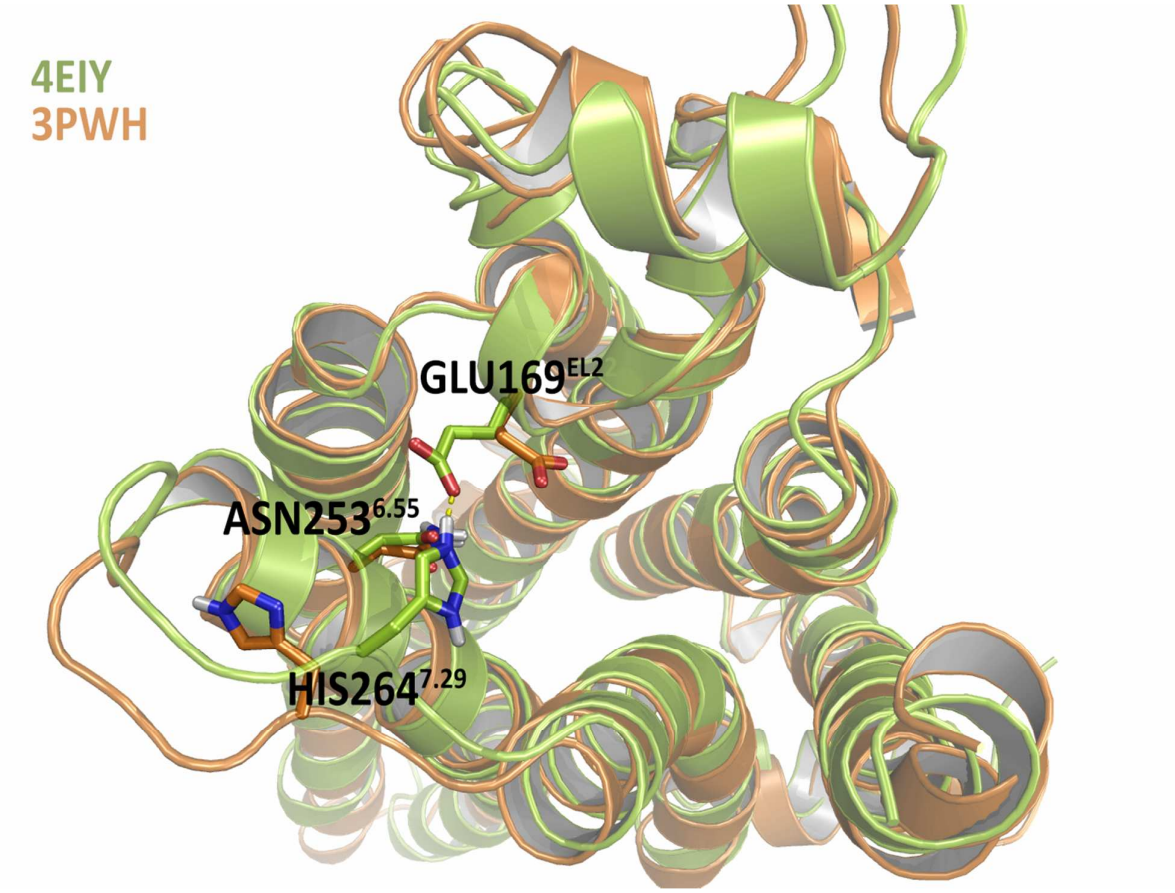

Figure S14. FEP map of the different perturbations, for the compounds of Figure 2, based on the crystal structure of 4EIY. Arrows between compounds represent the different perturbations. Red arrows highlight bad perturbations, based on hysteresis.

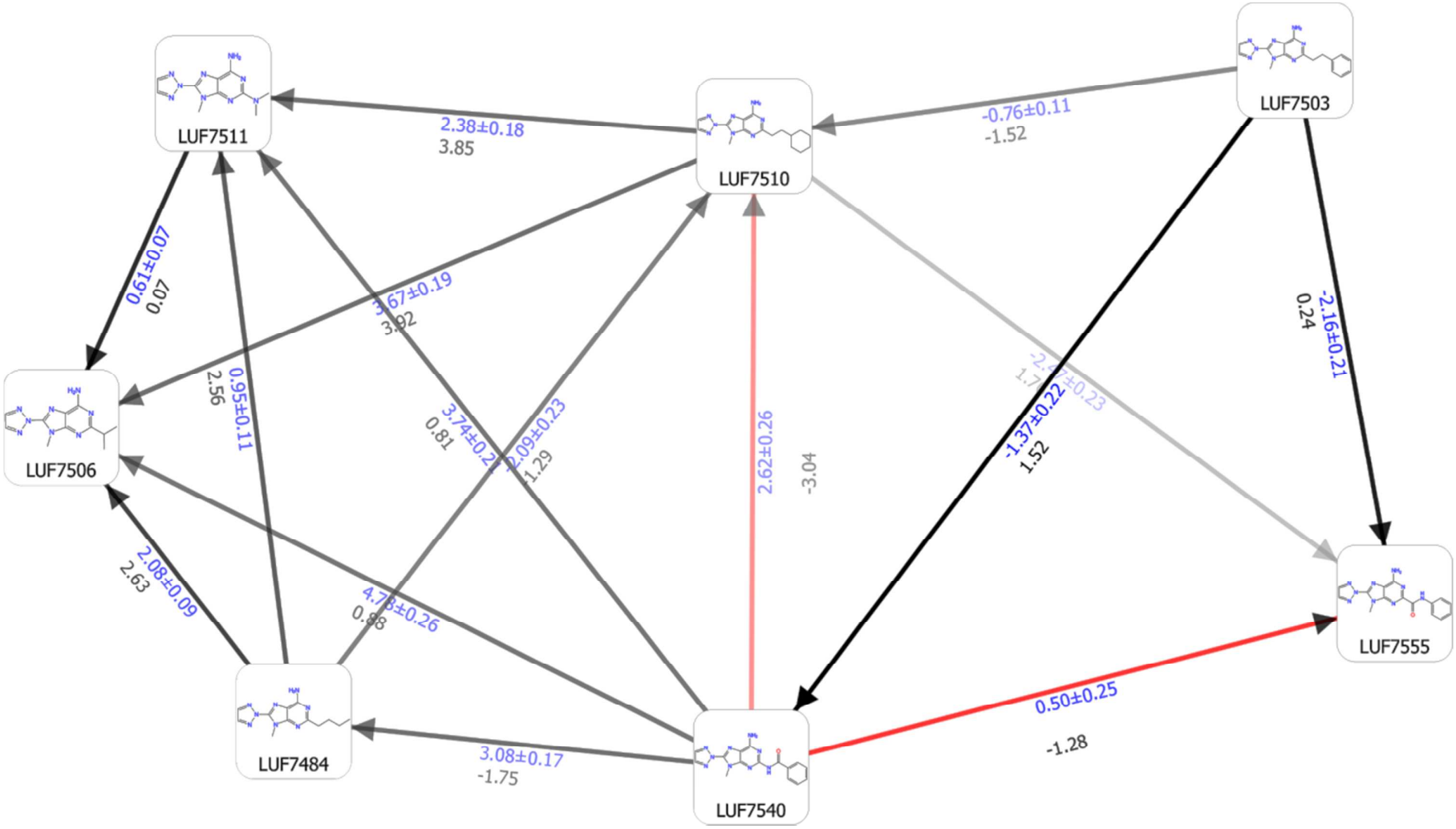

Figure S15. FEP map of the different perturbations, for the compounds of Figure 2, based on the crystal structure of 3PWH. Arrows between compounds represent the different perturbations. Red arrows highlight bad perturbations, based on hysteresis

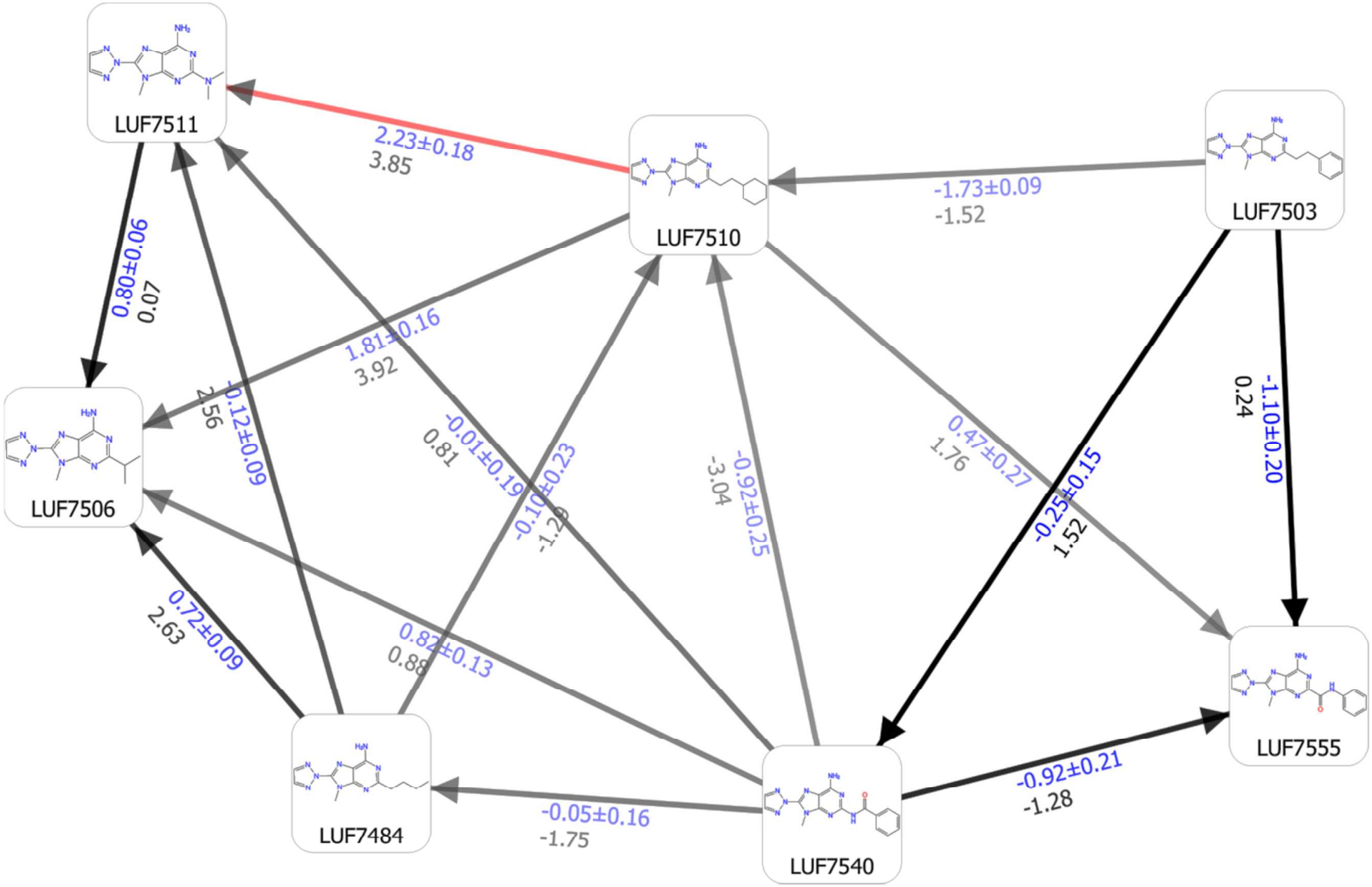

References

1. Small-Molecule Drug Discovery Suite 2014-3: Glide, version 6.4, Schrödinger, LLC, New York, NY, 2014.
2. Lyman, E.; Higgs, C.; Kim, B.; Lupyan, D.; Shelley, J. C.; Farid, R.; Voth, G. A., A Role for a Specific Cholesterol Interaction in Stabilizing the Apo Configuration of the Human A2A Adenosine Receptor. *Structure* **2009,** *17*, 1660-1668.
3. Piersanti, G.; Bartoccini, F.; Lucarini, S.; Cabri, W.; Stasi, M. A.; Riccioni, T.; Borsini, F.; Tarzia, G.; Minetti, P., Synthesis and Biological Evaluation of Metabolites of 2-n-Butyl-9-methyl-8-[1, 2, 3] triazol-2-yl-9 H-purin-6-ylamine (ST1535), A Potent Antagonist of the A2A Adenosine Receptor for the Treatment of Parkinson's Disease. *J. Med. Chem.* **2013,** *56*, 5456-5463.
4. Shivakumar, D.; Harder, E.; Damm, W.; Friesner, R. A.; Sherman, W., Improving the Prediction of Absolute Solvation Free Energies Using the Next Generation OPLS Force Field. *J. Chem. Theory Comput.* **2012,** *8*, 2553-8.
5. Harder, E.; Damm, W.; Maple, J.; Wu, C.; Reboul, M.; Xiang, J. Y.; Wang, L.; Lupyan, D.; Dahlgren, M. K.; Knight, J. L.; Kaus, J. W.; Cerutti, D. S.; Krilov, G.; Jorgensen, W. L.; Abel, R.; Friesner, R. A., OPLS3: A Force Field Providing Broad Coverage of Drug-like Small Molecules and Proteins. *J. Chem. Theory Comput.* **2016,** *12*, 281-96.
6. Minetti, P.; Tinti, M. O.; Carminati, P.; Castorina, M.; Di Cesare, M. A.; Di Serio, S.; Gallo, G.; Ghirardi, O.; Giorgi, F.; Giorgi, L., 2-n-Butyl-9-methyl-8-[1, 2, 3] triazol-2-yl-9 H-purin-6-ylamine and Analogues as A2A Adenosine Receptor Antagonists. Design, Synthesis, and Pharmacological Characterization. *J. Med. Chem.* **2005,** *48*, 6887-6896.
7. Thoma, G.; Streiff, M. B.; Kovarik, J.; Glickman, F.; Wagner, T.; Beerli, C.; Zerwes, H. G., Orally bioavailable isothioureas block function of the chemokine receptor CXCR4 in vitro and in vivo. *J. Med. Chem.* **2008,** *51*, 7915-20.
8. Yuan, Y.; Zaidi, S. A.; Elbegdorj, O.; Aschenbach, L. C.; Li, G.; Stevens, D. L.; Scoggins, K. L.; Dewey, W. L.; Selley, D. E.; Zhang, Y., Design, synthesis, and biological evaluation of 14-heteroaromatic-substituted naltrexone derivatives: pharmacological profile switch from mu opioid receptor selectivity to mu/kappa opioid receptor dual selectivity. *J. Med. Chem.* **2013,** *56*, 9156-69.
9. Christopher, J. A.; Brown, J.; Doré, A. S.; Errey, J. C.; Koglin, M.; Marshall, F. H.; Myszka, D. G.; Rich, R. L.; Tate, C. G.; Tehan, B., Biophysical fragment screening of the β1-adrenergic receptor: identification of high affinity arylpiperazine leads using structure-based drug design. *J. Med. Chem.* **2013,** *56*, 3446-3455.